Radially and azimuthally polarized non paraxial Bessel beams made simple

Marco Ornigotti,[1,*] **and Andrea Aiello**[1,2]

[1] *Max Planck Institute for the Science of Light, Günther-Scharowsky-Strasse 1/Bau24, 91058 Erlangen, Germany*
[2] *Institute for Optics, Information and Photonics, University of Erlangen-Nuernberg, Staudtstrasse 7/B2, 91058 Erlangen, Germany*
[*] *Corresponding author: marco.ornigotti@mpl.mpg.de*

Compiled January 15, 2013

We present a method for the realization of radial and azimuthal polarization for non-paraxial beams in a rigorous but simple manner. This is done by constructing independent exact vector solutions of Maxwell's equations from scalar Bessel beams and combining them together by analogy with the paraxial case. In this way we are able to obtain spatial and polarization patterns analogous to the traditional cylindrically polarized paraxial wave field. Applications of these beams are discussed.

OCIS codes: 260.0260, 260.5430, 260.6042

Among the broad zoology of solutions of Maxwell's equations, radially and azimuthally polarized vector beams, i.e., beams of light with non uniform polarization patterns, attracted great interest in the last decade [1–3]. Their particular character, in fact, makes them very appealing for applications in various fields of research such as single molecule spectroscopy [4], optical tweezing [5], confocal microscopy [6] as well as in commercial applications like material processing [7, 8] and data storage [9], just to name a few. Another interesting feature of such vector beams is that they can yield to very small focal spots [10] and generate axial electric [11] or magnetic [12] fields once focused. All these reasons have motivated the development of several experimental techniques to realize such field configurations [13–16]. Recently, it has been also shown that squeezed azimuthally polarized optical beams show hybrid entanglement [17]. For a comprehensive theoretical analysis of the properties (both classical and quantum) of general cylindrically polarized states of light, the reader is addressed to Ref. [18].

Despite the considerable amount of work that has been done in this field, radially and azimuthally polarized beams have been studied only within the framework of paraxial optics. The only exception, to the knowledge of the authors, is represented by the work of Bouchal and Olivik [19], where the concept of non-diffractive vector beam is introduced and extended to the non-paraxial domain. However, we feel that the physical meaning of the solutions found in Ref. [19] tends to be obscured by the use of a heavy mathematical formalism. It is our aim here to introduce cylindrically polarized states of light beyond the paraxial domain in a much simple way, by analogy with the paraxial case which leads to a clearer physical understanding, thus making this important subject accessible to a broader audience. Thanks to the fact that we use Bessel beams as basis to create these new fields, they will also possess the typical characteristics of Bessel beams, such as self healing and diffractionless propagation. They could also be used, as it has been recently proposed [20], to generate accelerating beams of arbitrary trajectories. All these features, combined with the complex cylindrical polarization pattern introduced here, may lead to new possible developments in timely research fields such as strongly focused light or to investigate the role of complex polarization patterns in light-atom scattering problems [21].

Let us start our analysis by considering a monochromatic scalar field $\psi(\mathbf{r})$ at angular frequency ω that is a solution of the scalar wave equation $(\nabla^2 + k^2)\psi(\mathbf{r}) = 0$, where $k = \omega/c$ is the wavenumber. It is not difficult to demonstrate [22] that the time-harmonic electric and magnetic vector fields are expressible in terms of the scalar field $\psi(\mathbf{r})$ as

$$\mathbf{E}(\mathbf{r}) = i\omega\left[\mathbf{A} + \frac{1}{k^2}\nabla(\nabla\cdot\mathbf{A})\right], \tag{1a}$$

$$\mathbf{B}(\mathbf{r}) = \nabla\times\mathbf{A}, \tag{1b}$$

where $\mathbf{A} = E_0\psi(\mathbf{r})\hat{\mathbf{f}}$, being $\hat{\mathbf{f}} = \alpha\hat{\mathbf{x}} + \beta\hat{\mathbf{y}}$, with $|\alpha|^2 + |\beta|^2 = 1$, is a complex unit vector orthogonal to the propagation axis z that defines the polarization of the beam and E_0 is arbitrary. For the sake of clarity, in the remaining part of the manuscript, we will focus our attention on the electric field solely.

As shown in Ref. [18], radially and azimuthally polarized beams live in a four dimensional space spanned by the basis formed by the Cartesian product of the base of Hermite-Gauss modes $\psi_{nm}(\mathbf{r})$ of order $N = n + m = 1$ [23] $\{\psi_{10}, \psi_{01}\}$ and the polarization basis $\{\hat{\mathbf{x}}, \hat{\mathbf{y}}\}$, namely $\{\psi_{10}, \psi_{01}\}\otimes\{\hat{\mathbf{x}}, \hat{\mathbf{y}}\} = \{\psi_{10}\hat{\mathbf{x}}, \psi_{10}\hat{\mathbf{y}}, \psi_{01}\hat{\mathbf{x}}, \psi_{01}\hat{\mathbf{y}}\}$. Linear combinations of these four vectors give rise to radially ($\hat{\mathbf{u}}_R$) and azimuthally ($\hat{\mathbf{u}}_A$) polarized fields as follows:

$$\hat{\mathbf{u}}_R^{\pm} = \frac{1}{\sqrt{2}}(\pm\psi_{10}\hat{\mathbf{x}} + \psi_{01}\hat{\mathbf{y}}), \tag{2a}$$

$$\hat{\mathbf{u}}_A^{\pm} = \frac{1}{\sqrt{2}}(\mp\psi_{01}\hat{\mathbf{x}} + \psi_{10}\hat{\mathbf{y}}), \tag{2b}$$

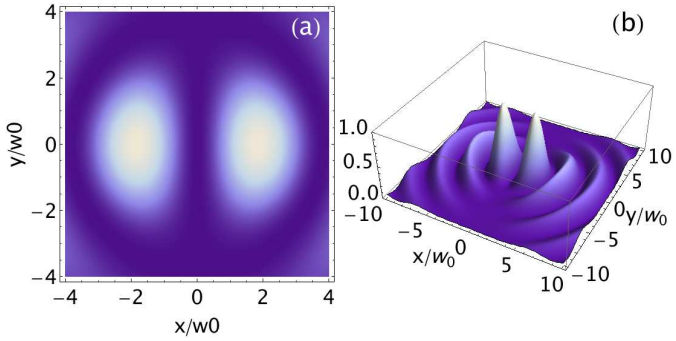

Fig. 1. Contour plot (a) and three dimensional intensity profile (b) of the scalar function $\Psi_{10}(\mathbf{r})$. Panel (a) shows how, close to the propagation axis, $\Psi_{10}(\mathbf{r})$ correctly reproduces the behavior of the Hermite-Gauss beam ψ_{10} employed in the paraxial case. Note from panel (b) that for $x/w_0 \geq 4$ and $y/w_0 \geq 4$, the scalar function $\Psi_{10}(\mathbf{r})$ shows some ripples, whose intensity is much smaller than the central lobes.

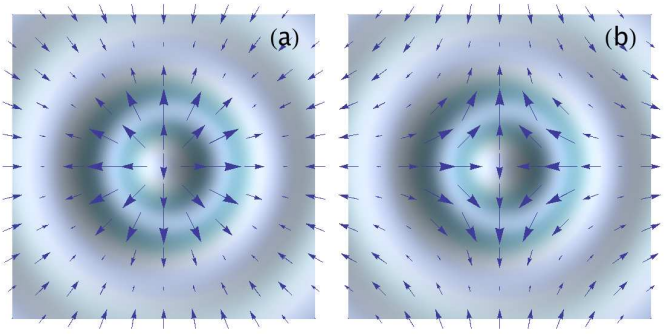

Fig. 2. Complex polarization patterns of (a) $\mathbf{U}_R^+$ and (b) $\mathbf{U}_R^-$, with superimposed the donut-shaped intensity distribution. The axes of both graphs span the interval $[-5, 5]$ in units of the beams waist w_0.

where the $\pm$ sign indicates co-rotating and counter-rotating modes respectively [18]. It is well known in paraxial optics that suitable linear combinations of Hermite-Gaussian modes may lead to orbital angular momentum carrying beams [24]. In particular, it is possible to demonstrate that the Hermite-Gauss modes ψ_{10} and ψ_{01} can be written as a superposition of two Laguerre-Gaussian beams with angular momentum $m = \pm 1$ [23].Having this in mind, we now construct the non-paraxial counterpart of the Hermite-Gaussian basis modes, using combinations of vector Bessel beams in such a way that the angular momentum of the resulting non-paraxial beam is preserved.

First, we choose for the scalar field a mth-order Bessel beam, namely $\psi_m^B(\mathbf{r}) = J_m(K_0 R)\exp(im\phi)\exp(iz\sqrt{k^2 - K_0^2})$, where $K_0 = k\sin\theta_0$ (being θ_0 the cone angle aperture of the Bessel beam), $x = R\cos\phi$ and $y = R\sin\phi$. Then we construct, by analogy with the paraxial case, the non paraxial scalar beams $\Psi_{10}(\mathbf{r})$ and $\Psi_{01}(\mathbf{r})$ by combining two Bessel beams $\psi_m^B(\mathbf{r})$ with angular momentum $m = \pm 1$ respectively, namely $\Psi_{10}(\mathbf{r}) = (\psi_1^B + \psi_{-1}^B)/\sqrt{2}$ and $\Psi_{01}(\mathbf{r}) = -i(\psi_1^B - \psi_{-1}^B)/\sqrt{2}$. In Fig. 1 the intensity profile of the scalar beam of $\Psi_{10}(\mathbf{r})$ is plotted as a function of the dimensionless coordinates x/w_0 and y/w_0 being $w_0 = 2/(k\theta_0)$ the beam waist. From this figure it is clear that, if we limit ourselves to the central domain (Fig. 1 (a)), the intensity distribution of the non paraxial beam $\Psi_{10}(\mathbf{r})$ is fully equivalent to the intensity distribution of the correspondent Hermite-Gauss beam ψ_{10}. Discrepancies start to arise in the non-centered region (Fig. 1 (b)), where the Hermite-Gauss beams are zero because of the Gaussian damping, while the beam $\Psi_{10}(\mathbf{r})$ presents ripples that have the symmetry structure of the central lobes, but a sensibly smaller intensity. The presence of these ripples is a signature of the non-paraxial character of these beams. As last step, following Eqs. (2) we build the non-paraxial radially and azimuthally basis as

$$\hat{\mathbf{U}}_R^{\pm} = \frac{1}{\sqrt{2}}\left(\pm\Psi_{10}\hat{\mathbf{x}} + \Psi_{01}\hat{\mathbf{y}}\right), \tag{3a}$$

$$\hat{\mathbf{U}}_A^{\pm} = \frac{1}{\sqrt{2}}\left(\mp\Psi_{01}\hat{\mathbf{x}} + \Psi_{10}\hat{\mathbf{y}}\right). \tag{3b}$$

These modes are *exact* vector solutions of the full Helmholtz equation, since the scalar fields $\Psi_{10}(\mathbf{r})$ and $\Psi_{01}(\mathbf{r})$ are solutions of the full Helmholtz equation, in contrast with the case of Gaussian beams that are solution of the paraxial equation solely. However, they are not exact solutions of Maxwell's equations, as they do not evidently satisfy the transversality condition $\nabla \cdot \hat{\mathbf{U}}_{R,A}^{\pm} = 0$. Exact solutions of the Maxwell's equations are obtained by substituting $\hat{\mathbf{U}}_R^{\pm}$ and $\hat{\mathbf{U}}_A^{\pm}$ into the right side of Eq. (1), to generate electric and magnetic fields that are automatically satisfying the condition $\nabla \cdot \mathbf{E}(\mathbf{r}) = 0$.

The polarization pattern as well as the intensity distributions of these non-paraxial radially and azimuthally polarized beams are displayed in Figs. 2 and 3. Although they retain their typical donut-like intensity distribution, a closer inspection of the polarization pattern of these beams reveals that they possess a nonzero longitudinal field component, as can be understood by noting that, in contrast to their paraxial counterpart (see Ref. [18]) they manifest a nonzero polarization in correspondence with the center of the intensity distribution. The intensity distributions of these non paraxial vector beams are displayed in Fig. 4 for both the cases of radially (upper panels) and azimuthally (lower panels) polarized beams. In particular, the panels (b) and (d) show the intensity distribution of the longitudinal component of such beams. As can be seen, for the radially polarized beam the z-component of the electric field different from zero, although about three orders of magnitude less intense

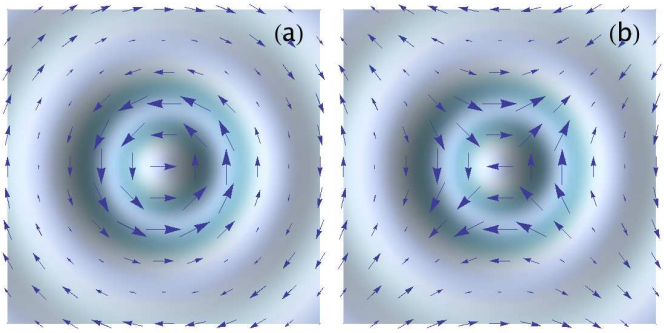

Fig. 3. Complex polarization patterns of (a) $\mathbf{U}_A^+$ and (b) $\mathbf{U}_A^-$,with superimposed the donut-shaped intensity distribution. The axes of both graphs span the interval $[-5, 5]$ in units of the beams waist w_0.

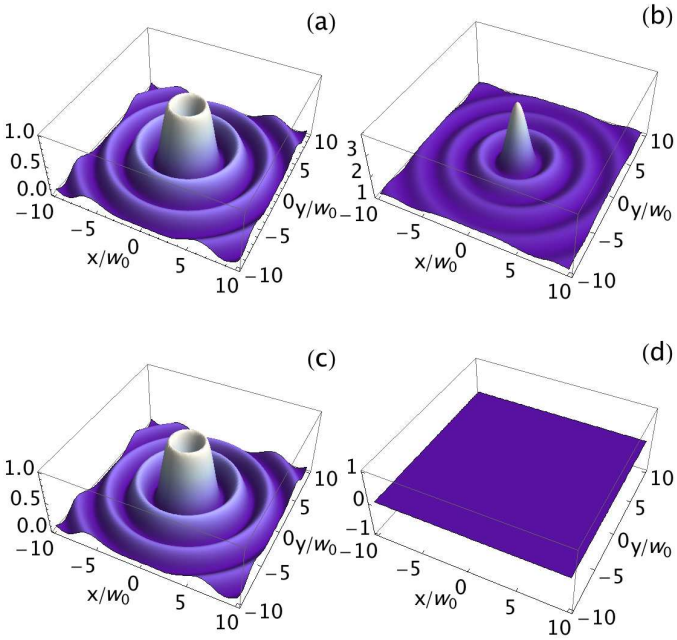

Fig. 4. Intensity distributions for the radially (upper row) and azimuthally (lower row) polarized non paraxial electromagnetic fields. Panels (a) and (c) display the transversal components of the field $(|E_x|^2 + |E_y|^2)$, while in panels (b) and (d) the longitudinal component $|E_z|^2 \times 10^4$ is depicted. The coordinates are expressed in units of w_0. The intensity of the z-component of the electric field has been rescaled to the maximum of the transverse intensity distribution.

than the transversal intensity distribution. On the other hand, the z-component of the electric field for the azimuthally polarized beam (panel (d)) remains exactly zero.

In conclusion, we have shown how to generalize the theoretical framework of radially and azimuthally polarized beams to the case of non-paraxial fields, using Bessel beams as generating beams. We shown that these non-paraxial fields retain the typical donut-shape of their paraxial counterparts, although they show a nonzero longitudinal electric field component for the case of radially polarized beams.

References

1. C. J. R. Sheppard, J. Opt. Soc. Am. A **17**, 335 (2000)
2. C. Maurer, A. Jesacher, S. Fürhapter, S. Bernet and M. Ritsch-Marte, N. J. Phys. **9**, 78 (2007)
3. R. Martinez-Herrero, P. M. Mejias and G. Piquero, *Characterization of Partially Polarized Light Fields*, Springer (2009)
4. B. Sich, B. Hecht and L. Novotny, Phys. Rev. Lett. **85**, 4482 (2000)
5. M. Sondermann, R. Maiwald, H. Konermann, N. Lindlein, U. Peschel and G. Leuchs, Appl. Phys. B **89**, 489 (2007)
6. N. Huse, A. Schönle and S. W. Hell, J. Biomed. Opt. **6**, 273 (2001)
7. A. V. Nesterov, V. G. Niziev and V. P. Yakunin, Appl. Opt. **29**, 2234 (1990)
8. M. Meier, V. Romano and T. Feurer, Appl. Phys. A **86**, 329 (2006)
9. B. Van Waeyenberge, A. Puzic, H. Stoll, K. W. Chou, T. Tyliszczak, R. Hertel, M. Fähnle, H. Brückl, K. Rott, G. Reiss, I. Neudeckr, D. Weiss, C.H. Back and G. Schütz, Nature **444**, 461 (2006).
10. R. Dorn, S. Quabis and G. Leuchs, Phys. Rev. Lett **91**, 233901 (2003)
11. S. Quabis, R. Dorn, M. Eberler, O. Glöckl and G. Leuchs, Opt. Comm. **179**, 1 (2000)
12. J. R. Zurita-Sanchez and L. Novotny, J. Opt. Soc. Am. B **19**, 2722 (2002)
13. T. Grosjean, A. Sabac and D. Courjon, Opt. Comm **252**, 12 (2005)
14. K. C. Toussaint, Jr. S. Park, J. E. Jureller and N. F. Scherer, Opt. Lett. **30**, 2846 (2005)
15. Z. Bosmon, V. Kleiner and E. Hasman, Appl. Phys. Lett. **79**, 1587 (2001)
16. K. J. Moh, X.-C. Yuan, J. Bu, R. E. Burge and B. Z. Gao, Appl. Opt. **46**, 7544 (2007)
17. C. Gabriel, A. Aiello, W. Zhong, T.G. Euser, N. Y. Joly, P. Banzer, M. Förtsch, D. Elser, U. L. Andersen, Ch. Marquardt, P. St. J. Russel and G. Leuchs, Phys. Rev. Lett. **106**, 060502 (2011)
18. A. Holleczek, A. Aiello, C. Gabriel, Ch. Marquardt and G. Leuchs, Opt. Expr. **19**, 9714 (2011)
19. Z. Bouchal and M. Olivik, J. Mod. Opt. **42**, 1555 (1995)
20. I. D. Chemmos, Z. Chen, D. N. Christodoulides and N. K. Efremidis, Opt. Lett. **37**, 5003 (2012)
21. M. Ornigotti and A. Aiello, in preparation
22. J. D. Jackson, *Classical electrodynamics*, Wiley (1999)
23. M. J. Padgett and J. Courtial, Opt. Lett. **24**, 430 (1999)
24. L. Allen, M. W. Beijersbergen, R. J. C. Spreeuw and J. P. Woerdman, Phys. Rev. A **45**, 8185 (1992)